Molecular Crystals and Liquid Crystals
Publication details, including instructions for authors and subscription information:
http://www.tandfonline.com/loi/gmcl20

# Synthesis, Growth and Characterization of 1H-Benzimidazolium Hydrogen L-Tartrate Dihydrate Single Crystals

M. Rajalakshmi [a], R. Indirajith [a], P. Ramasamy [b] & R. Gopalakrishnan [a]

[a] Department of Physics, Anna University, Chennai, 600025, India

[b] Centre for Crystal Growth, SSN College of Engineering, Kalavakkam, Tamilnadu, India

Version of record first published: 07 Oct 2011

To cite this article: M. Rajalakshmi, R. Indirajith, P. Ramasamy & R. Gopalakrishnan (2011): Synthesis, Growth and Characterization of 1H-Benzimidazolium Hydrogen L-Tartrate Dihydrate Single Crystals, Molecular Crystals and Liquid Crystals, 548:1, 126-141

To link to this article: http://dx.doi.org/10.1080/15421406.2011.590374

*Mol. Cryst. Liq. Cryst.*, Vol. 548: pp. 126–141, 2011

ISSN: 1542-1406 print/1563-5287 online
DOI: 10.1080/15421406.2011.590374



# Synthesis, Growth and Characterization of 1H-Benzimidazolium Hydrogen L-Tartrate Dihydrate Single Crystals

M. RAJALAKSHMI,[1,*] R. INDIRAJITH,[1] P. RAMASAMY,[2] AND R. GOPALAKRISHNAN[1]

[1]Department of Physics, Anna University, Chennai 600025, India
[2]Centre for Crystal Growth, SSN College of Engineering, Kalavakkam, Tamilnadu, India

*The 1H-Benzimidazolium Hydrogen L-Tartrate Dihydrate (BT) was synthesized using benzimidazole and L-tartaric acid and grown as single crystal by slow evaporation solution growth technique at room temperature (RT) using double-distilled water as a solvent. The crystal system has been confirmed from the single crystal X-ray diffraction (XRD) and powder XRD analyses. Morphology of the grown BT crystal was obtained using WinXMorph software package. Photoluminescence (PL) and UV–Visible (UV–Vis) spectral studies were performed. The functional groups present in the material were identified from Fourier transform infrared (FT-IR) spectroscopy. The thermal stability of the crystal was studied by TG-DTA (Thermalgravimetry analysis and Differential Thermal Analysis). The dielectric behavior was analyzed both as a function of frequency and temperature. The mechanical strength of the grown crystal was studied with Vickers microhardness tester. The growth patterns were analyzed after etching the surface of the crystal. The second harmonic generation (SHG) of BT was tested by Kurtz–Perry powder technique.*

**Keywords** Characterization; growth from solution; nonlinear optical materials; single crystal growth; X-ray diffraction

## 1. Introduction

Organic nonlinear optical (NLO) materials have attracted considerable research attention for their potential applications in many fields, such as information storage, optical communications, and optical chemistry. In the last decade, Zyss et al. [1] have introduced octupolar model for second order nonlinear optics. Second order nonlinear optical materials are at the heart of telecommunication devices, such as electro-optic modulators and optical switches, and in lasers, such as high power green and blue solid state lasers and optical parametric amplifiers. The 1H-Benzimidazolium Hydrogen L-Tartrate Dihydrate (BT) possess the property of both positive and negative sides of amino acids.] The charge carriers of Benzimidazole are similar to that of amino acids but, unlike $NH_3^+$ sites of amino acids,

*Address correspondence to R. Gopalakrishnan, Department of Physics, Anna University, Chennai 600025, India. Tel.: +91-44-2235 8710/8707; Fax: +91-44-2235 8700. E-mail: krgkrishnan@annauniv.edu, krgkrishnan@yahoo.com

benzimidazolium has delocalized electron clouds. Its carboxylic group of BT properties are same as that of amino acid itself. Hence, we attempted the synthesis of BT.

## 2. Experimental Details

### *2.1. Synthesis, Solubility and Growth of BT*

The title compound was synthesized by taking Benzimidazole and L-Tartaric acid in an equimolar ratio. Benzimidazole was dissolved in methanol and L-Tartaric acid was dissolved in distilled water in separate beakers. The two separately prepared clear solutions were mixed together and stirred well by using magnetic stirrer. The obtained curd like product was dried in an oven at 60°C. The chemical reaction of BT is shown in Fig. 1. The reaction between Benzimidazole and L-Tartaric acid can be written as below:

$$C_7H_6N_2 + C_4H_6O_6 \rightarrow C_7H_7N_2^+.C_4H_5O_6^-.2H_2O$$

According to Fig. 1, there is electrostatic attraction between nitrogen carriers (the positive charge) and $COO^{--}$ of tartaric acid. A cation and anion interaction takes place, where the cation again acts as a crosslink between adjacent anionic aggregates. The two water molecules provide an additional six hydrogen bonds thereby generating a complex three-dimensional (3D) hydrogen-bonded network throughout the structure [2].

The solubility of BT in various solvents like ethanol, methanol, water, and N–N dimethyl formide (DMF) was carried out. BT was found to be well dissolved in water and DMF. Double-distilled water is chosen as a suitable solvent for crystal growth. The solubility of BT was estimated from room temperature (RT) to 45°C in steps of 5°C. A volume of 50 ml of water was taken in a beaker and known quantity of synthesized product of BT was added till saturation is obtained. The temperature of the solution was maintained at chosen temperature in constant temperature bath. The solution was continuously stirred using motorized magnetic stirrer to ensure homogenous temperature and concentration throughout the entire volume of the solution. The solubility of BT increases with increasing temperature; it shows the positive solubility coefficient as shown in Fig. 2.

The slow evaporation solution growth method was employed to grow BT crystals. From the solubility data, the required amount of synthesized BT material was dissolved in 100 ml of double distilled water and stirred well for 1 hr to attain the homogenous mixture. The saturated solution was filtered using Whatman filter paper and closed tightly with polythene sheet to control the evaporation of the solvent. The solution was housed in constant temperature bath at RT. The slow evaporation of the solvent yielded good transparent bulk crystals over a time span of three months. A Crystal of size 27 mm × 5 mm was successfully grown as shown in Fig. 3(a).

## 3. Characterization

### *3.1. X-ray Diffraction (XRD) Analysis*

The single crystal XRD data of BT crystal were collected using Nonius CAD4/MACH 3 single crystal X-ray diffractometer, using $MoK_\alpha$ radiation ($\lambda = 0.71073$ Å). It is observed that the crystal belongs to the monoclinic system with noncentrosymmetric space group $P2_1$. The obtained crystallographic data are presented in Table 1 and the values are in good agreement with the reported values. In addition, the powder XRD pattern was recorded

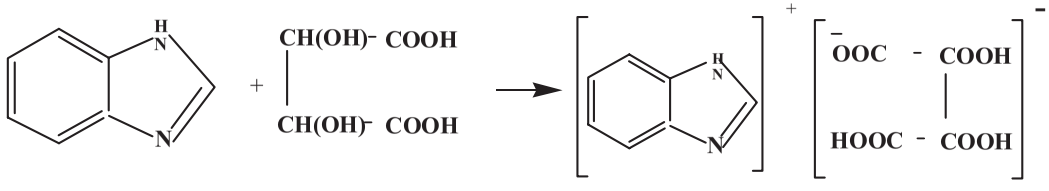


**Figure 1.** Reaction between Benzimidazole and L-Tartaric acid.

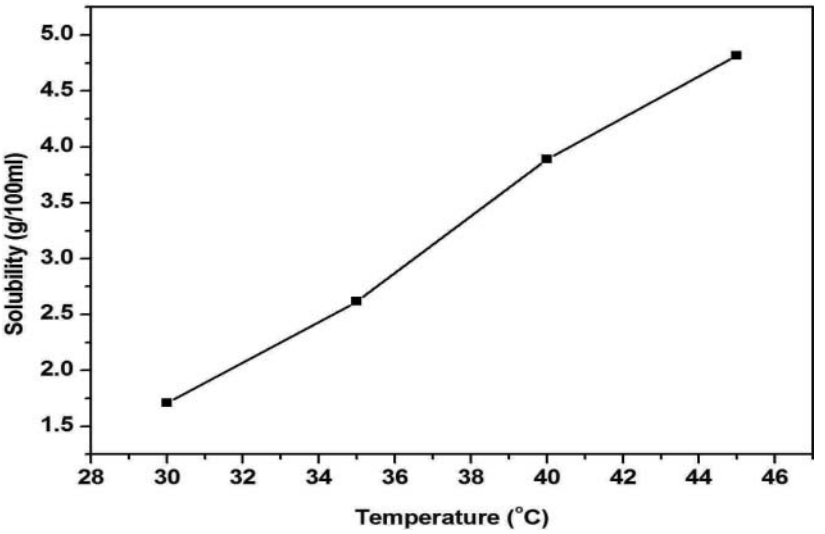


**Figure 2.** Solubility of 1H-Benzimidazolium Hydrogen L-Tartrate Dihydrate (BT).

using Rich–Seifert powder X-ray diffractometer with $CuK_\alpha$ radiation ($\lambda = 1.5428$ Å). The sample was scanned in the $2\theta$ values ranging from 10° to 50° at the rate of 3°/min. The obtained peaks were indexed using the PROZSKI software package. The recorded powder XRD spectrum of BT is shown in Fig. 4. Crystal morphologies are predicted from data stored in files in the common intermediate format (CIF format, crystallographic information file standard of the International Union of Crystallography) on the basis of the Bravais–Friedel, Donnay–Harker model [3]. CIF and powder XRD data are given as input and the morphology diagram was drawn for BT crystal using WinXMorph software as shown in Fig. 3(b).

### *3.2. FT-IR Spectra*

The FT-IR analysis of BT was carried out to investigate the presence of functional groups and their vibrational modes. The spectrum was recorded in the region 4000–400 $cm^{-1}$ using Perkin–Elmer Spectrum RX1 spectrophotometer equipped with He–Ne source, KBr beam

**Table 1.** Crystallographic data of BT

| Lattice parameter | Present study | Reported values [2] |
|---|---|---|
| A | 9.222(2) Å | 9.2181(1) Å |
| B | 7.282(1) Å | 7.279(2) Å |
| *c* | 10.945(2) Å | 10.957(3) Å |
| $\beta$ | 110.30(2)° | 110.43(2)° |
| V | 689.4(3) $Å^3$ | 689.0(3) $Å^3$ |
| System | Monoclinic | Monoclinic |
| Space group | $P2_1$ | $P2_1$ |

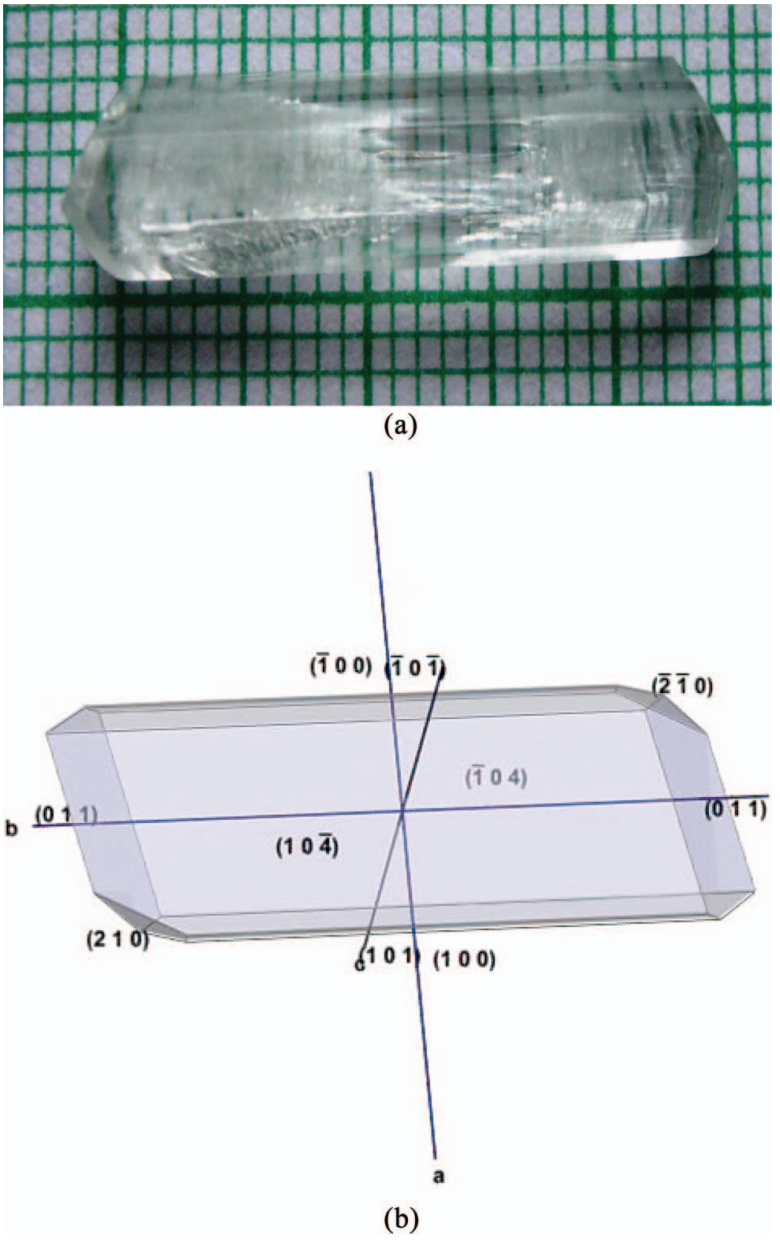


**Figure 3.** (a) As grown BT single crystal using double distilled water as a solvent, and (b) morphology diagram of BT single crystal obtained using WinXMorph software.

splitter and $LiTaO_3$ detector. The sample was prepared by mixing it with KBr into pellet form. The recorded spectrum is shown in Fig. 5. The intense broadband between 2100 $cm^{-1}$ and 3400 $cm^{-1}$ is due to O–H of Tartrate [4,5]. The broadening is due to hydrogen bonding. The sharp peak at 3146 $cm^{-1}$ is assigned to N–H vibration of benzimidazole moiety. The signal at 3086 $cm^{-1}$ is due to aromatic C−H vibration of benzimidazole. It is the characteristic one to confirm the presence of benzimidazole in the crystal lattice. The C−H

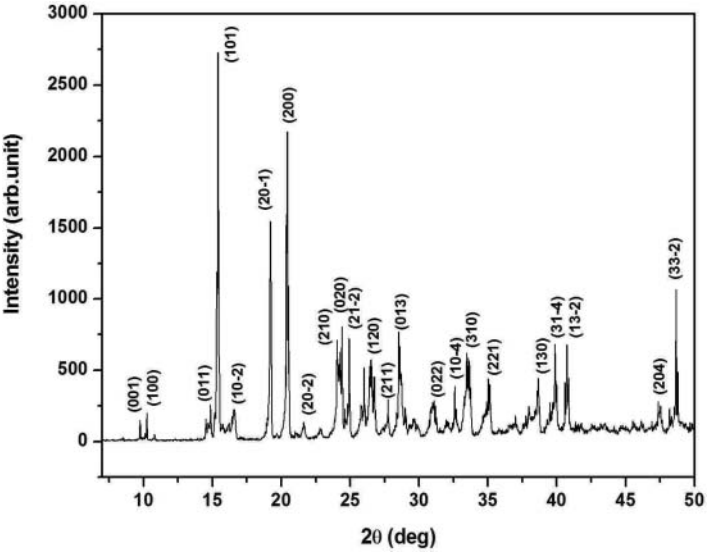


**Figure 4.** Powder XRD pattern of BT.

vibration of tartrate gives its peak at 2198 $cm^{-1}$. The C=O vibration of $COO^-$ in tartrate gives its peak at 1663 $cm^{-1}$. In free tartaric acid, C=O vibration occurs at 1736 $cm^{-1}$ [6]. The shift toward low value, therefore, illustrates the transfer of carboxylic proton to carboxylic acid benzimidazole. Presence of benzimidazole in the crystal is once again verified by the characteristic ring vibration at about 1600 $cm^{-1}$ and 1410 $cm^{-1}$ [7]. The peak at 1316 $cm^{-1}$ is due to C−H bending. The C−O vibration of −COOH of tartaric acid gives its peak at 1081 $cm^{-1}$ and 979 $cm^{-1}$. The group of peaks below 1000 $cm^{-1}$ is due to C−H bending modes of benzimidazole ring [5].

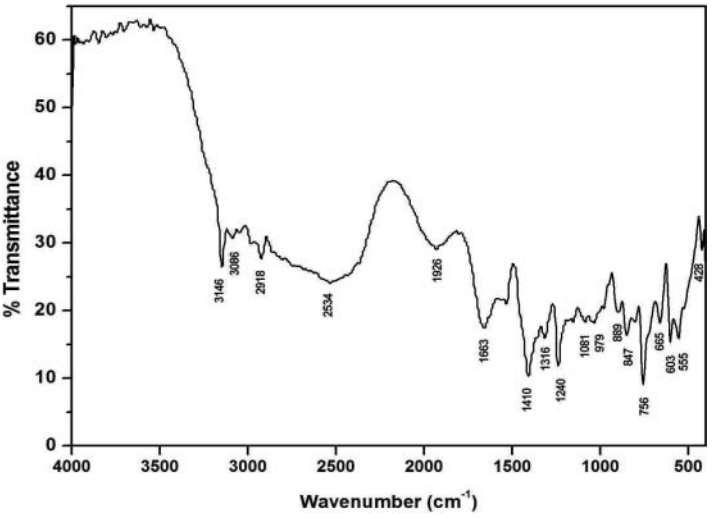


**Figure 5.** FT-IR pattern of BT.

### *3.3. Optical Transmittance Studies*

The transmittance and absorbance spectra of the title crystal were recorded using the Perkin–Elmer Lambda 35 UV–Visible (UV–Vis) spectrometer in the region 250–850 nm. The plots of transmittance (%) with wavelength (nm) and absorbance with wavelength, shown in Fig. 6, were obtained with a crystal of thickness 2 mm. NLO material can be of utility only if it has a wide transparency window without any absorption at the fundamental and second harmonic wavelengths and preferably with the lower limit of transparency window being well below 400 nm. The UV–Vis range from 200 nm to 400 nm is very important for the realization of second harmonic generation (SHG) output in this range using diode and solid–state lasers [8]. In Fig. 6(a) the transmittance increases exponentially from the UV–Vis region toward the visible region and gives the transmittance of about 88% in the visible region. The cut-off wavelength of BT is at 280 nm. From the graph, it is evident that the crystal has a transparency window from 374 nm suggesting the suitability of BT for SHG. From the absorbance spectrum, it is observed that crystal absorbs heavily within UV–Vis region but moderately in the Visible–Near infrared (Vis–NIR) region. The absorbance spectrum of the BT crystal is shown in Fig. 6(b).

*3.3.1 Optical Band Gap.* Optical band gap of the material was calculated from the transmittance spectrum. The measured transmittance ($T$) was used to calculate the absorption coefficient ($\alpha$) using the formula,

$$\alpha = \frac{2.3026\log\left(\frac{1}{T}\right)}{t} \tag{1}$$

where, $t$ is the thickness of the sample.

The optical band gap ($E_g$) was evaluated from the transmission spectrum and the optical absorption coefficient ($\alpha$) near the absorption edge is given by the Tauc's equation (2) [9,10]

$$h\upsilon\alpha = A(h\upsilon - E_g)^m \tag{2}$$

where, $A$ is a constant, $\alpha$ is the optical absorption coefficient, $h$ is Planck's constant, $\nu$ is the frequency of the incident photon, $E_g$ is the optical band gap, and $m$ is a constant which characterizes the nature of band transition. Among all possible transitions, $m = 1/2$ is found to more suitable for BT crystal since it gives the best linear curve in the band edge and hence the transition is direct allowed. The band gap was calculated from the plot between $h\nu$ and $(\alpha h\nu)^{1/2}$ as shown in the Fig. 6(c). The value of $E_g$ is found to be 4.0 eV. The materials thus exhibited high transmittance of 70%–80% in the visible region and has wide optical band gap of 4.0 eV. Hence, it may be a good candidate for the optical application.

*3.3.2 Refractive Index (n).* The refractive index of the material can be measured from the reflectance of the material. The reflectance ($R$) in terms of the absorption coefficient can be obtained from equation (3) [11].

$$R = \frac{\exp(-\alpha t) \pm \sqrt{\exp(-\alpha t)T - \exp(-3\alpha t)T + \exp(-2\alpha t)T^2}}{\exp(-\alpha t) + \exp(-2\alpha t)T} \tag{3}$$

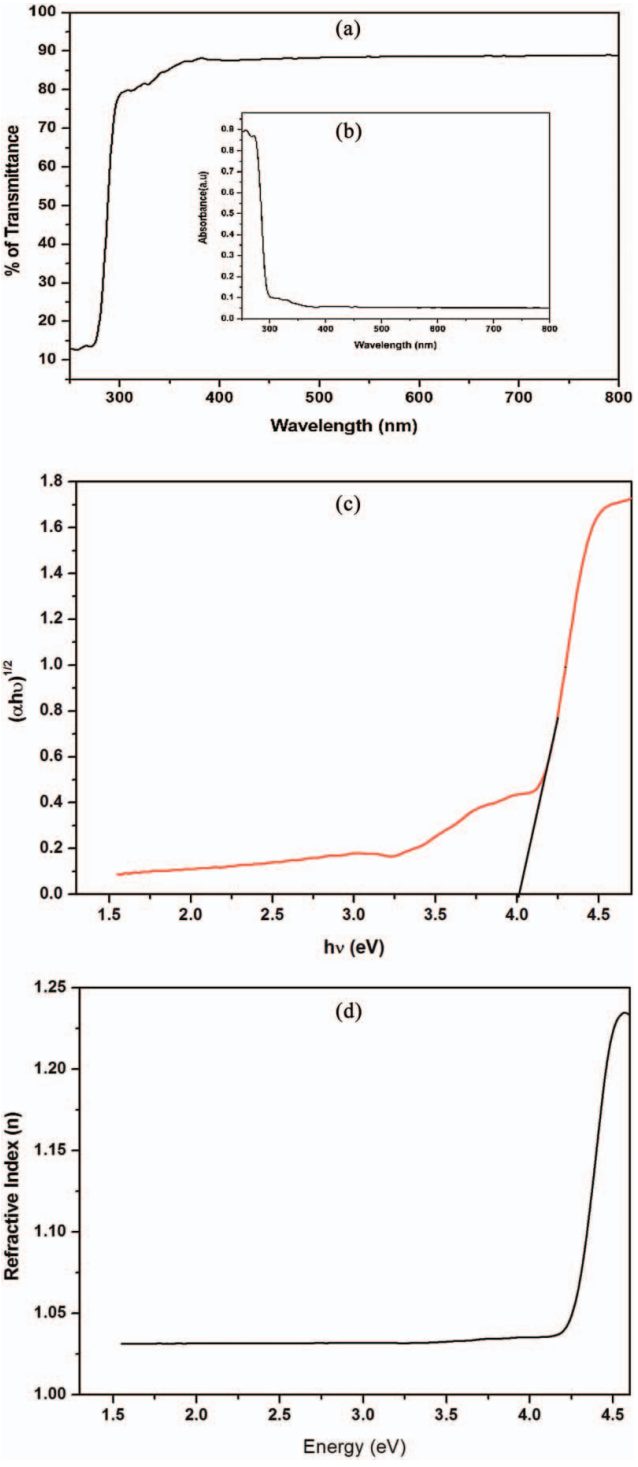


**Figure 6.** (a) Transmittance spectrum of BT crystal and inset, (b) Absorbance spectrum, (c) Plot of photon energy versus $(\alpha h\nu)^{1/2}$ for BT crystal, and (d) Plot of variation of photon energy with refractive index of BT crystal.

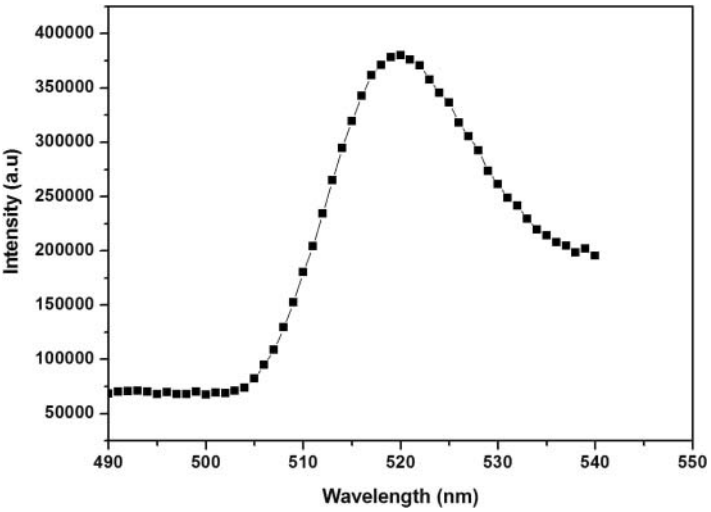


**Figure 7.** PL spectrum of BT crystal.

The refractive index ($n$) can be determined from reflectance data using

$$n = \frac{-(R+1) \pm 2\sqrt{R}}{(R-1)} \tag{4}$$

The variation of refractive index ($n$) with photon energy is shown in Fig. 6(d) for BT crystal. The refractive index ($n$) decreases with increasing wavelength. Benzimidazole carriers delocalized electronic cloud interaction between the electronic cloud and photon is the cause for change in the refractive index. The refractive index ($n$) is 1.23 at 4.12 eV for BT crystal.

### *3.4. Photoluminescence (PL) Studies*

PL is the spontaneous emission of light from a material under optical excitation. PL investigations can be used to characterize a variety of material parameter. The PL spectrum was recorded using a Jobin Y Van–Spex Spectrofluorometer (Fluorolog version-3. Model/FL3-11) with the excitation wavelength of 230 nm consisting of a silicon photodiode, a photomultipler tube (PMT) for PL detection, highpressure xenon arc, which is operated at 150/450 watts. Excitation and emission spectra were obtained by changing the excitation wavelength under a fixed emission wavelength and vice versa. The recorded PL spectrum of BT crystal is shown in Fig. 7. The greenish yellow emission band gave a maximum at 520 nm (2.38 eV). The broadening of emission band is due to lattice vibrations in the BT crystal. Lattice vibrations caused by thermal vibrations of atoms due to temperature changes. There are three basic classes of defects in crystals, like point defect, linear defect, and planar defect [12]. Impurities occur because materials are never 100% pure. In the case of an impurity, the atom is often incorporated at a regular atomic site in the crystal structure. The atom is neither on a vacant site nor an interstitial site. The atom is not supposed to be anywhere in the crystal, and is thus an impurity. The emission was assigned to electronic transition from $\pi^*$ antibonding molecular orbital to $\pi$ bonding molecular orbital of benzimidazole. The low intense photoluminescence behaviors observed above

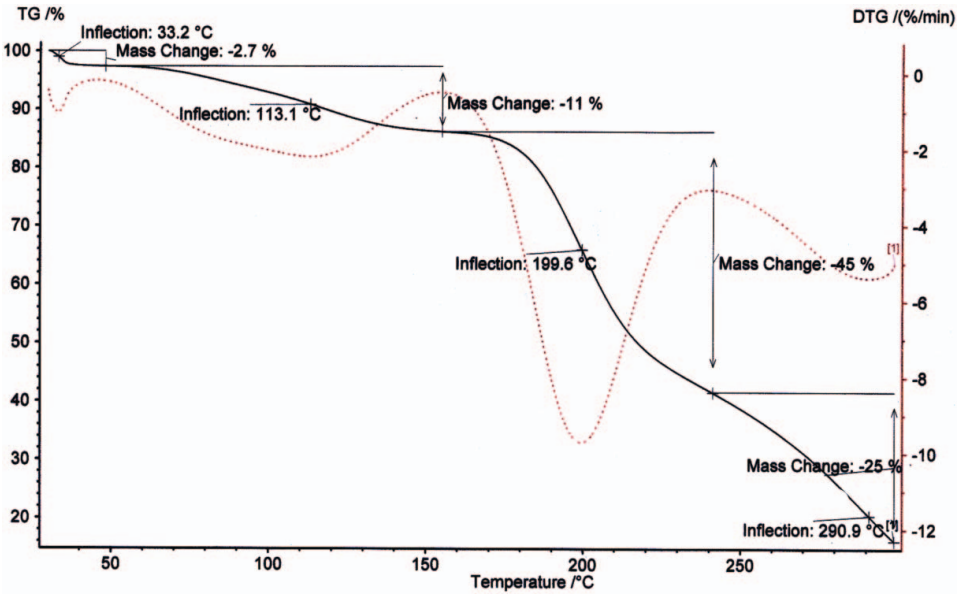


**Figure 8.** DTA and TGA curves of BT.

620 nm in the higher wave number region substantiate large hydrogen bonded association of benzimidazole in the crystal lattice.

### *3.5. Thermogravimetric Analysis (TGA)*

The thermal stability of BT was identified by the TGA and differential thermal analyses (DTA) using a NETZSCH STA 409 C/CD thermal analysis system between the temperatures 30°C and 300°C at a heating rate of 10°C/min in nitrogen atmosphere in the alumina crucible. The TGA and DTG results are illustrated in Fig. 8. There is some minute weight loss of about 2.7% below 50°C owing to less physically absorbed water. The weight loss that extends from 60°C–150°C is assigned to loss of water of crystallization. The 11% weight loss indicates 2 moles of water as water of crystallization of salt. A major weight loss starts from 160°C due to degradation of BT. The degradation occurs in two stages. From the above analysis, it is concluded that the crystal can be applied for NLO application up to of 60°C.

The derivatives of DTA and TGA of BT are illustrated in Fig. 9. A minute endotherm appearing below 40°C is assigned to the loss of physically absorbed water. It is followed by two major endotherms with origin at about 70°C both endotherms origin to loss of water of crystallization. It is also coinciding with the weight loss between 60°C and 160°C. At about 150°C, there is a sharp endotherm that is assigned to melting point of BT. The melting point was determined using a melting point apparatus, and it is found to be 154°C, thus confirming that the endotherm is due to melting and followed by degradation.

### *3.6. Dielectric Studies*

The dielectric measurements were made using HIOKI 3635 model LCR meter in a frequency range 100 Hz–5 MHz at different temperatures ranging from RT to 70°C. This system is

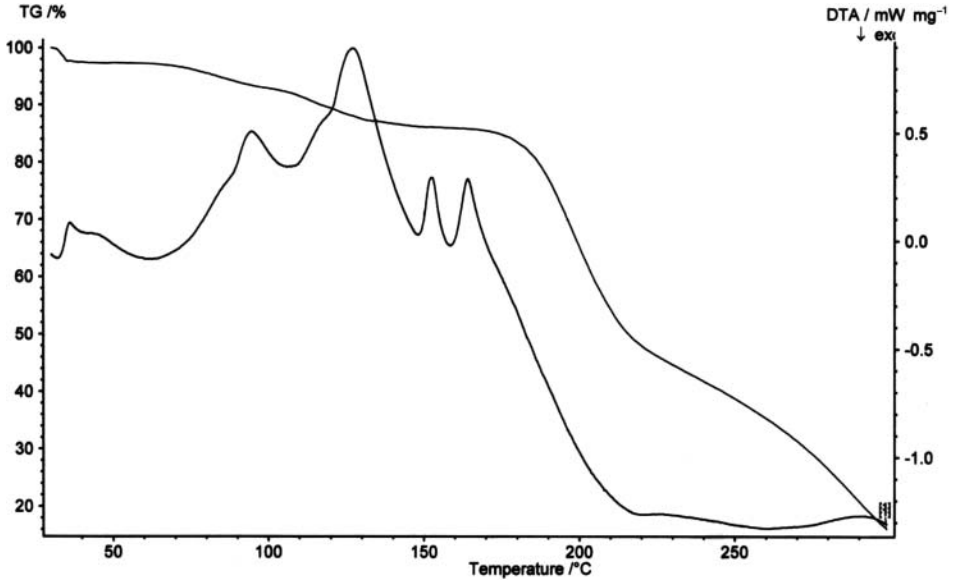


**Figure 9.** Derivatives of DTA and TGA of BT.

automated using a computer for data recording, storage, and analysis. Desired sizes of grown single crystals were selected and they were polished with a soft tissue paper for measurement. The sample was electroded by applying silver paste on opposite faces to make a capacitor for measurement. A small cylindrical furnace was used to house the sample to determine the dielectric constant at different temperatures, whose temperature is controlled by temperature controller with accuracy of $\pm 0.01^{\circ}$C. The dielectric constant ($\varepsilon'$) and dielectric loss ($\varepsilon'$) were calculated from the values of $C$ and $t$ using the relation

$$\varepsilon' = \frac{Ct}{\varepsilon_0 A} \tag{5}$$

where, $C$ is the capacitance; $A$ is the area of cross section of the crystal; $t$ is the thickness of the sample, and $\varepsilon_0$ is the dielectric constant in vacuum. Variation of dielectric constant with frequency at different temperatures for BT crystal is shown in Fig. 10. From the graph, it is observed that the value of dielectric constant is high at low frequency and decreases exponentially with increasing frequency for various temperatures, above 1.77 MHz, the dielectric constant remains same. The magnitude of $\varepsilon_r$ depends on the degree of polarization of charge displacement in the crystals. The dielectric constant of a material is contributed by four types of polarization mechanisms, namely ionic, electronic, orientational, and space charge polarization, which depends on the frequency of the ac voltage applied across the material [13].

At low frequency, all these polarizations are active but the space charge polarization is active at lower frequencies and high temperatures [14]. The space charge polarization will depend on the purity and perfection of the material, and its influence is large at high temperatures. The decrease in the value of $\varepsilon_r$ with the frequency is observed when the jumping frequency of electric charge carriers cannot follow the alternation of the ac electric field applied beyond a certain critical frequency. As the frequency increases, at which the space charge cannot sustain and comply the external field. Therefore, the polarization

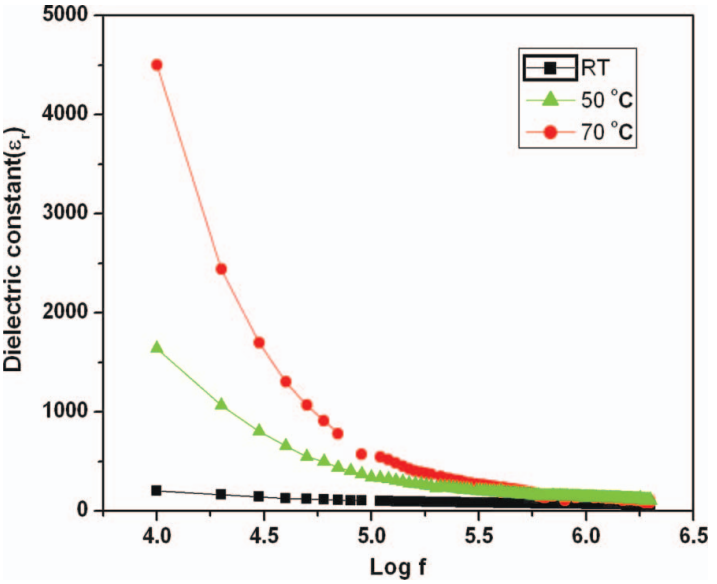


**Figure 10.** Variation of dielectric constant with log frequency.

decreases and exhibiting the reduction in the value of dielectric constant with increasing frequency.

The variation of dielectric loss with log *f* is measured for the crystal as shown in Fig. 11. From the graph, it is observed that the dielectric loss is less at high frequencies and increases exponentially at low frequencies. As the frequency increases, the space charge cannot sustain at a point and comply with the external field and hence the polarization decreases

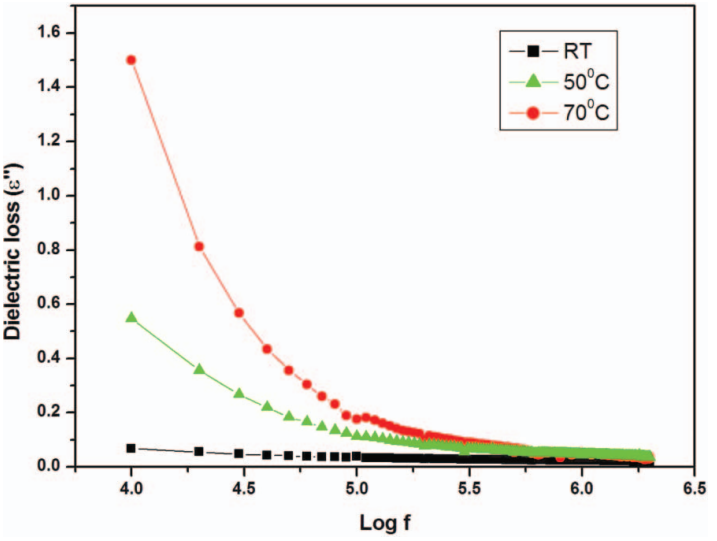


**Figure 11.** Variation of dielectric loss with log frequency.

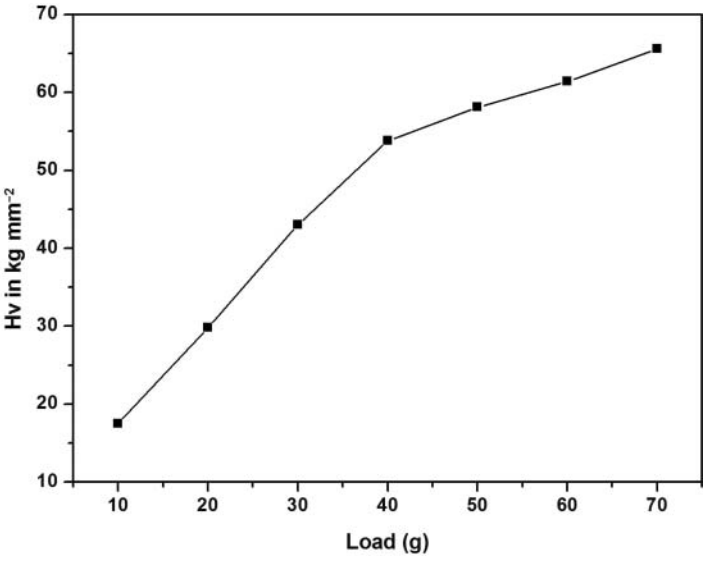


**Figure 12.** Variation of Vicker's Hardness with load.

giving rise to diminishing values of $\varepsilon''$. The low value of dielectric loss indicates good quality of the crystal (with fewer defects) [15].

### *3.7. Hardness Studies*

Microhardness of a crystal is its capacity to resist indentation. Physically hardness is the resistance offered by a material to localized deformations caused by scratching or by indentations [16,17]. The mechanical strength of the grown crystal in the plane (1 0 $\bar{4}$) was found out using Reichert MD 4000E ultra microhardness tester fitted with a Vickers diamond pyramidal indenter. The indentations were made at RT with a constant indentation time of 5 s. The diagonal length of the indentation impression was measured using a microscope. In order to get accurate results for each applied load, several indentations were made on the sample and the average diagonal length ($d$) of the indenter impressions were measured. The Vicker's microhardness number Hv of the crystal was calculated using the equation

$$\mathrm{Hv} = 1.8544P/d^2(\mathrm{kg/mm^2}) \tag{6}$$

where, $P$ is the applied load and $d$ is the mean diagonal length of the indenter impression. Hardness measurements were taken for applied loads 10–60 g keeping the time of indentation constant at 5 s for all the cases. The relation between Vicker's microhardness number and applied load for BT is shown in Fig. 12. It is observed that the Vicker's microhardness value increases with the applied load. Test load above 60 g develops multiple cracks on the crystal surface due to the release of internal stress generated locally by indentation. It is observed from the measurement that the microhardness value increases with increasing load.

The work hardening coefficient value ($n$) of the grown crystal was determined from the plot of log $P$ versus log $d$ by least square fit method (Fig. 13). According to Onitsch [18] if

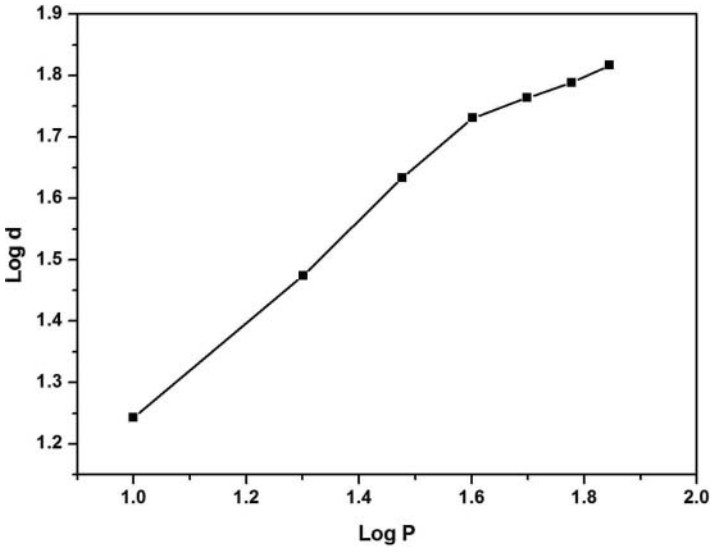


**Figure 13.** Plot of Log P versus Log d.

$n > 2$, the microhardness number Hv increases with increasing load. The work hardening coefficient ($n$) is found to be more than 2, which proves that BT crystal belongs to soft material.

### *3.8. Etching Studies*

The nonlinear efficiency of the NLO material mainly depends on the quality of the grown crystals because the segregated impurities and dislocations occur during growth results in the distortion of the optical beam to be processed. Hence, it is very essential to study the microstructural imperfections or crystal defects in the grown crystals [19]. In the present experimental work, transparent crystal free from inclusions and cracks was selected in the plane $(10\bar{4})$. Etching of the crystal surface was carried out by dipping the crystal in distilled water for a few seconds at RT for 5, 10, and 20 s and then wiped it with dry filter paper. Water is a superior etching solution for revealing dislocation etch pits and it is insensitive to surface orientation as it produced pits almost on all surfaces [20]. Etch patterns were observed and photographed under an optical microscope in the reflected light. Fig. 14(a) shows the surface features of the as-grown BT single crystal before etching and the linear etch patterns observed for 5, 10, and 20 s are shown in Figs 14(b)–(d), respectively. The size of the pits increases with the increase of etching time while the pit pattern remains same. The observed etch pits, due to layer growth, confirmed the two-dimensional nucleation (2D) mechanism with less dislocations [21]. The surface micrograph shows that the growth on the $(1\ 0\bar{4})$ plane takes place predominately by two-dimensional layer growth.

### *3.9. Kurtz–Perry Powder SHG Test*

The determination of SHG intensity of the crystals using powder technique was developed by Kurtz and Perry [22]. The sample was prepared by grinding the crystal into fine crystalline powder and packed in the capillary tube. The powder sample of BT was illuminated by

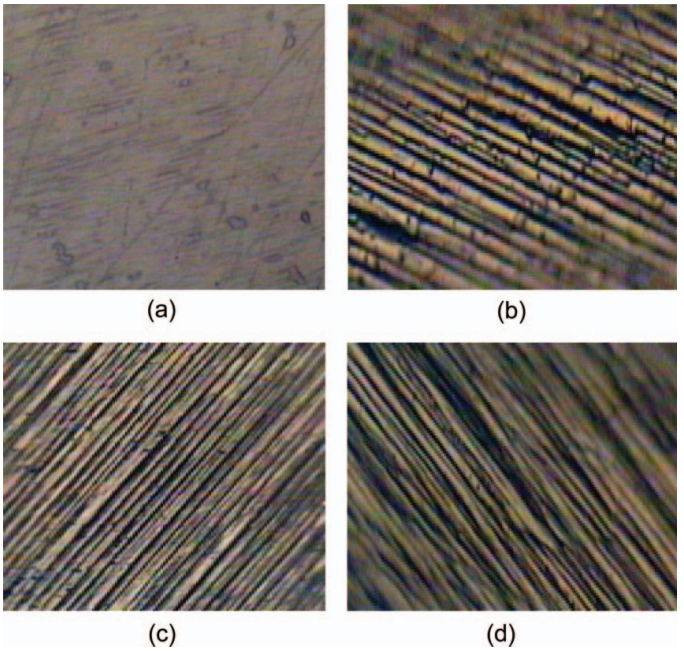


**Figure 14.** Etch pit patterns of BT single crystal with water as an etchant in the plane $(10\bar{4})$ (a) before etching, (b) 5 s, (c) 10 s, and (d) 20 s.

the laser source ($\lambda = 1064$ nm). The second harmonic signal generated in the sample was collected by the lens and detected by the monochromator, which is coupled with the photomultiplier tube. The bright green emission was observed from the output of the powder form of the BT ($\lambda = 532$ nm). KDP sample was used as reference material. The output power intensity of BT was comparable with the output power of KDP and it was 1.2 times with the output power of KDP.

## 4. Conclusions

The BT has been synthesized and grown as single crystal by slow evaporation solution growth technique at RT. The single crystal XRD and powder XRD studies confirm that the BT crystal belongs to monoclinic system with space group $P2_1$. The functional groups present in the grown crystal have been confirmed by FT-IR spectral analysis. The optical study reveals high transparency of BT crystal in the entire visible region. The optical band gap ($Eg = 4.0$ eV) and refractive index ($n$) of the material were calculated from the transmittance spectrum. The broad greenish yellow emission is centered at 2.38 eV in PL spectrum. The thermal analyses reveal good thermal stability of the material thereby proving its suitability for NLO applications. Surface micrographs recorded reveal that BT crystal grows by two-dimensional layer growth mechanisms.

## References

[1] Zyss, J., & Ledoux, I. (1994). *Chem. Rev.*, *94*, 77–105.
[2] Aakeroy, B. C., & Hitchcock, B. P. (1994). *Acta Cryst.*, *C50*, 759–761.

[3] Kaminsky, W. (2007). *J. Appl. Cryst.*, *40*, 382–385.
[4] Vogel, A. I., Tatchell, A. R., Furnis, B. S., Hannaford, A. J., & Smith, P. W. G. (1989). *Vogel's Textbook of Practical Organic Chemistry*, 5th Edition, ELBS: England.
[5] Silverstein, R. M., & Webster, F. X. (1998). *Spectrometric Identification of Organic Compounds*, 6th Edition, John Wiley Eastern & Sons: Canada.
[6] Martin Britto Dhas, S. A., Suresh, M., Bhagavannarayana, G., & Natarajan, S. (2007). *J. Cryst. Growth*, *309*, 48–52.
[7] Vijayan, N., Ramesh Babu, R., Gopalakrishnan, R., & Ramasamy, P. (2004). *J. Cryst. Growth*, *262*, 490–498.
[8] Dmitriev, V. G., Gurzadyan, G. G., & Nikoyosyan, D. N. (1999). *Hand Book of Nonlinear Optical Crystals*, 3rd edition, Springer: Berlin.
[9] Mott, N. F., & Gurney, R. W. (1940). *Electronic Processes in Ionic Crystals*, 2nd Edition, Oxford: London.
[10] Tauc, J. (1974). *Amorphous and Liquid Semiconductors*, Plenum: New York.
[11] Anandha babu, G., & Ramasamy, P. (2009). *J. Cryst. Growth, 311*, 1185–1189.
[12] Callistar, D. W. (2007). *Materials Science and Engineering an Introduction*, 7th Edition, John-Wiley &Sons: New York.
[13] Babu, R. R., Sethuraman, K., Vijayan, N., Bhagavannarayana, G., Gopalakrishnan, R., & Ramasamy, P. (2006). *Cryst. Res. Technol.*, *41*, 906–910.
[14] Prasad, N. V., Prasad, G., Bhimasankaran, T., Suryanarayana, S. V., & Kumar, G. S. (1969). *Indian J. Pure Appl. Phys.*, *14*, 639.
[15] Charles, J. B., & Gnanam, F. D. (1994). *Cryst. Res. Technol.*, *29*, 707–712.
[16] Subhadra, K. G., Rao, K. K., & Sirdeshmukh, D. B. (2000). *Bull. Mater. Sci.*, *23*, 147–150.
[17] Mukerji, S., & Kar, T. (1999). *Cryst. Res. Technol.*, *34*, 1323–1328.
[18] Onitsch, E. M. (1947). *Mikroscopia*, *2*, 131–151.
[19] Mukerji, S., & Kar, T. (1999). *Jpn. J. Appl. Phys.*, *38*, 832–837.
[20] Mukerji, S., & Kar, T. (1999). *J. Cryst. Growth*, *200*, 543–549.
[21] Mukerji, S., & Kar, T. (1999). *J. Cryst. Growth*, *204*, 341–347.
[22] Kurtz, S. K., & Perry, T. T. (1968). *J. Appl. Phys.*, *39*, 3798–3813.